Discontinuous shear thickening in concentrated suspensions

Georges Bossis, Olga Volkova, Yan Grasselli, Oumar Gueye, Alain Ciffreo

PHILOSOPHICAL TRANSACTIONS A

Phil. Trans. R. Soc. A.
doi:10.1098/not yet assigned

Discontinuous shear thickening in concentrated suspensions

Georges Bossis[1], Olga Volkova[1],Yan Grasselli[1,2],Oumar Gueye[1],Alain Ciffreo[1]

[1]Laboratory Inphyni, Institute of Physics of Nice,CNRS, University of Nice Sophia-Antipolis, Nice, France
[2]Université Côte d'Azur – SKEMA Business School – 60 rue Dostoievski – CS30085 – 06902 Sophia Antipolis, France

Keywords: Discontinuous shear thickening, jamming,magnetotheology, suspension ,stick slip,paste extrusion

Summary

The flow of concentrated suspensions of solid particles can be suddendly blocked by the formation of a percolated network of frictionnal contacts above a critical value of the applied stress. Suspensions of magnetic particles coated with a superplastifier molecule were shown to produce a strong jamming transition. We find that, for these supensions with an abrupt discontinuous shear thickening , a model using a divergence of the viscosity at a volume fraction which depends on the applied stress does not well describe the observed behavior both below and above the critical stress. At a constant applied stress above the critical one, we have a stick slip behavior of the shear rate whose period can be predicted and scales as the square root of the relaxation time of the frictional contacts. The application of a small magnetic field allows to continuously decrease the critical shear rate and it appears that the yield stress induced by the magnetic fiekd does not contribute to the jamming transition. At last it is shown that this jamming transition also appears in the extrusion of the suspension through a die, but with a much slower dynamics than in the case of stress imposed on a rotational geometry.

Introduction

The shear thickening is an increase of viscosity with the shear rate contrary to a Newtonian fluid where the viscosity remains constant whatever the shear rate. In colloidal suspensions it is frequent to observe this shear thickening which is interpreted as due to the formation of aggregated flocs under the increase of the shear force between particles which overcomes the potential barrier due to a coating polymer or an ionic layer. These flocs emprison the suspending liquid which then behave as a solid of the size of the floc. The result is an increase of the effective volume fraction and so of the viscosity. A model of this mechanism was described in (1), (2). In hard sphere suspension where there are only hydrodynamic interactions, the viscosity does not depend on the shear rate and diverges at a maximum volume fraction Φ_{max} which is close to the maximum random close packing: Φ_{RCP}=0.64:

$$\eta(\Phi) = \eta_0 \left(1 - \frac{\Phi}{\Phi_{max}}\right)^{-p} \qquad (1)$$

*Author for correspondence (Bossis@unice.fr).
†Present address: Inphyni,CNRS,UCA,Parc Valrose,06108,Nice

where p is an. exponent close to 2. Actually the experiments made in order to find the value of the exponent p and of Φ_{max} suffer from inaccuracies related to the polydispersity, non negligible short range interactions, uncertainty in the measurement of volume fraction etc..

In colloidal suspensions the thermodynamic stresses, which scale as kT/a^3 -where a is the radius of the particles-are far from being negligible and are responsible for a first shear thinning behavior before a shear thickening one due to the formation of hydroclusters when hydrodynamic forces dominate at large Peclet number (3). Non Brownian suspensions are obtained with particles whose radius is typically larger than one micron. Still in these suspensions, sedimentation and Van der Waals forces are present and combine to provoke the agregation of the particles if they are not coated with a polymer layer which generates an entropic repulsive force between the adsorbed layers on the surface of the particles. In these supensions formed with non Brownian particles, a shear thickening is observed when the volume fraction is increased (typically above 50%) and above a critical volume fraction, this continuous shear thickening (CST) is replaced by a discontinuous one (DST), which appears as a decrease of the shear rate in a stress imposed ramp, or as a jump in stress in a shear rate imposed ramp. In a well monodisperse suspension this transition was shown to be due to the disparition of an ordered structure, formed of hexagonal planes sliding over each other ,above a critical stress able to destroy it (4), (5). Nevertheless this DST behavior also happens in suspensions where the distribution of particles is far from being monodisperse and can also have irregular shape as is the case with the well known cornstarch suspension (6), (7) .Many other systems based on silica (8), (9), gypsum (10), poly-methylmethacrylate (11), calcium carbonate (12), (13) etc.also show this jamming transition. There is some large evidence, supported by numerical simulation (14) and also by AFM measurement of forces between particles (15) , that this transition is related to the passage from lubricated contacts to frictional ones when the shear force increases enough to overcome the potential barrier formed by a stabilizing layer. The critical shear force needed to produce this transition depends on the characteristic of the adsorbed layer of polymer. For instance we have shown that, for the same particles, we can observe a difference of critical stress by a factor of three by changing the superpastifier and we have related this difference to the amplitude of the repulsive force generated by the different polymers (13). If it is interesting in industrial processing of pastes to be able to repel this jamming transition at the highest possible value of stress by a proper choice of the coating polymer, it would be still more interesting to be able to control the critical stress by an external mean. That is what we have succeeded to do by using suspensions of magnetic particles whose interaction forces can be modulated by the application of a magnetic field (16). Indeed the critical shear rate is shown to decrease strongly with the amplitude of the magnetic field and contrarily to the expectation, the critical stress is not constant but increases with the magnetic field.

In a first part , we shall present some typical rheological behavior associated with the jamming transition and we shall adapt the model of Wyart and Cates (17) in the presence of a yield stress and discuss the ability of this model to represent this transition. In a second part we shall more specifically address the control of the jamming transition with a magnetic field and we shall try to understand why the critical stress increases in the presence of a magnetic field. The third section will be devoted to the study of the instabilities which occur in the regime of flow in the jammed state and the last section to a preliminary study of the jamming transition during the extrusion of the suspension through a die

Rheological characteristics of the jamming transition

When the volume fraction of a suspension of non Brownian particles is increased, the rheogram, as represented by the shear stress versus the shear rate will change progressively, passing from a quasi Newtonian behavior to a shear thickening one and finally will end up with the jamming transition as represented in Fig.(1).

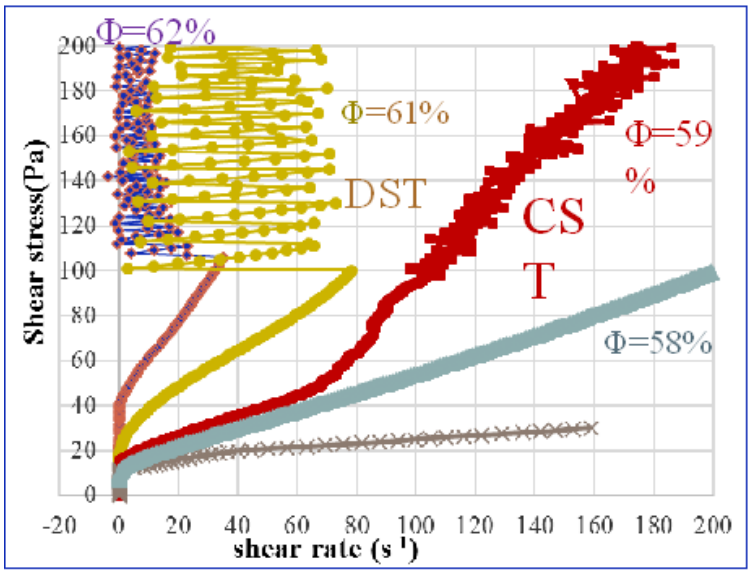

Fig.1 Evolution of the rheology of a suspension of calcium carbonate in water in the presence of the PPP44 molecule

The rheograms are obtained on a rheometer MCR 501 (Anton Paar) in a plate plate geometry, the ramp of stress is made at typically 50Pa/mn which is slow enough to guarantee the absence of thixotropy (13). The suspension is made of particles of calcium carbonate (Omnya) in water where we have added 0.2% in mass of a superplastifier molecule which is a polyoxyethlene polyphosphonate used in the cement industry. This molecule strongly adsorbs on the calcium sites of the particles through the PO_3^{--} phosphonate ionic groups of the molecule. The polyoxyethylene tail is composed in average of 44 oxyethylene groups: CH2-CH2-O, which has a quite good affinity with water (13); in the following we shall call this molecule PPP44. We see that even at a volume fraction as high as 58% the yield stress τ_y is quite low (around 15Pa) and that the dynamic viscosity is constant, so the whole rheogram is well represented by a Bingham law: $\tau = \tau_v + \eta_d \dot{\gamma}$. At Φ =59% the behavior is already quite different with a strong increase of the viscosity above a shear rate of 60 s^{-1}, followed by a domain with small oscillations. Then at Φ=61% we have a strong jamming transition with a sudden decrease of the shear rate followed by a regime of strong oscillations around 35s^{-1}. Finally, at 62% there is also a jamming transition but occurring at a lower shear rate. If we still increase the volume fraction, at some given value close to 68% the system is completely jammed and there is no flow at all when the stress is increased. Actually a definitive blocking of the system whatever the imposed stress will depend a lot of the plasticity of the particles, of the roughness of the walls of the cell, and of the non-dilatancy of the gap under large applied shear stress.

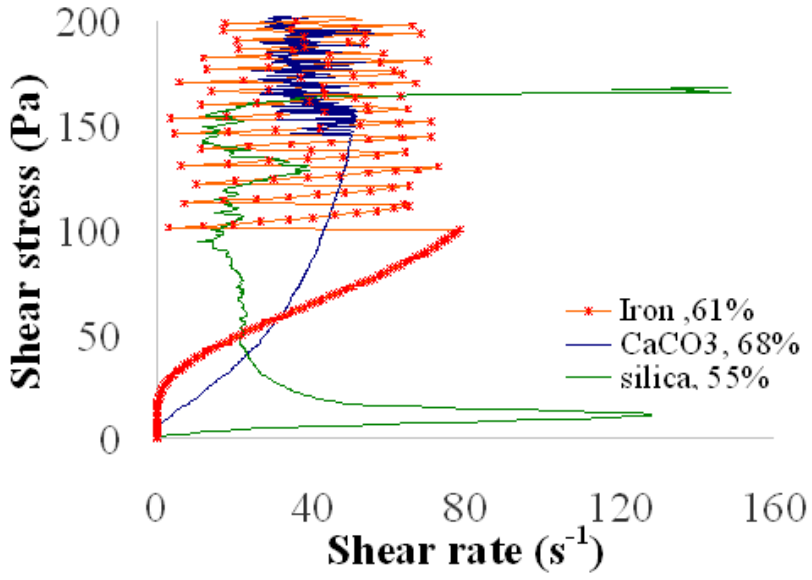

Fig.2 Jamming transition for suspensions composed of iron particles (red symbols), Carbonate calcium particles (solid blue line) and silica particles (solid green line)

The DST transition can be more or less abrupt. For instance, in Fig.2 we have reported the jamming transition for carbonyl iron particles (average diameter 1.2µm), for carbonate calcium particles (average diameter 4µm), and for silica particles average diameter 5µm). The three suspensions are in water but the two first ones are stabilized by 0.2% in mass of the molecule PPP44 whereas there is no surfactant with silica whose stabilization is due to its natural ionization in water. The iron particles present the stronger transition with, above the critical shear stress τ_c=100Pa, large fluctuations of the shear rate -we shall come back to this point in the third section. The calcium carbonate at Φ=68% has also an abrupt transition for τ_c =147Pa but followed by some much smaller oscillations of the shear rate. Last, for the suspension of silica particles there is a continuous decrease of the shear rate above τ_c=12Pa but without a clear regime of oscillation. Note also that the abrupt increase of shear rate at τ=165 Pa is just due to the expulsion of the suspension out of the gap between the two plates. It is worth noting that other systems

do not show a decrease of the shear rate but only a stop of the increase which corresponds to a vertical line, on the stress-shear rate graph; this is the case for cornstarch suspension in water or silica particles in mineral oil (18). These different regimes depend likely on the deformability of the particles and on the softness of the repulsive barrier formed by a coating polymer or an ionic layer.

In Figs (1) and (2), the rheogram correspond to a ramp of shear stress that is to say to a continuous increase of the torque on the upper plate. In this situation, a transformation of the suspension in a jammed state can produce a decrease of the rotation speed or even its complete stop. On the other hand, if the motor imposes a ramp of velocity, when the shear rate exceeds the critical one, we expect a jump in the shear stress which will recover, if it exists, the branch where the shear rate begins again to increase in the regime of imposed stress. Actually, in the suspensions with an abrupt jamming transition, the jump of stress above the critical shear rate, is very high and well above the rheometer maximum torque. Furthermore, the stress generated is transmitted radially and ejects the particles outside the suspension (19). In a plate-plate geometry the suspension goes out of the gap while in cylindrical Couette geometry particles are pushed outside the free surface and air enters the suspension, producing a foam at the surface. In order to get rid of a free interface and also to have a high enough torque capacity, we have used a high torque viscosimeter developed by CAD company, mainly to measure the viscosity of concrete. We have designed a cell where the suspension is confined by a teflon seal (Fig.3a). To prevent slipping we have used either a vane or a double helix as the rotating tool; also the outside wall is serrated with stripes of depth 0.2mm. This rheometer works in the imposed velocity mode and in Fig 3b we have reported the stress measured during a ramp of shear rate. We see that there is an abrupt jump of stress which reaches 80kPa, nevertheless this stress does not remain at this high level but oscillates between the flowing and a jamming state which increases with the shear rate. In this case, the structure of the suspension manages to come back transiently to the flowing state despite the fact that the shear rate is above the critical one. We shall discuss this point in the section devoted to the application of a magnetic field.

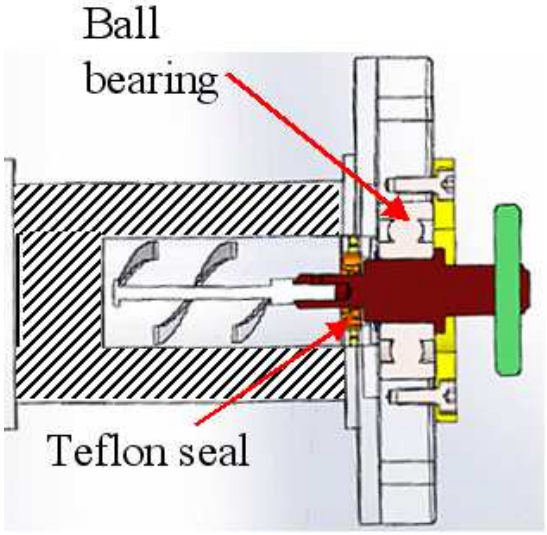

Fig.3a Schematic of the confined cell

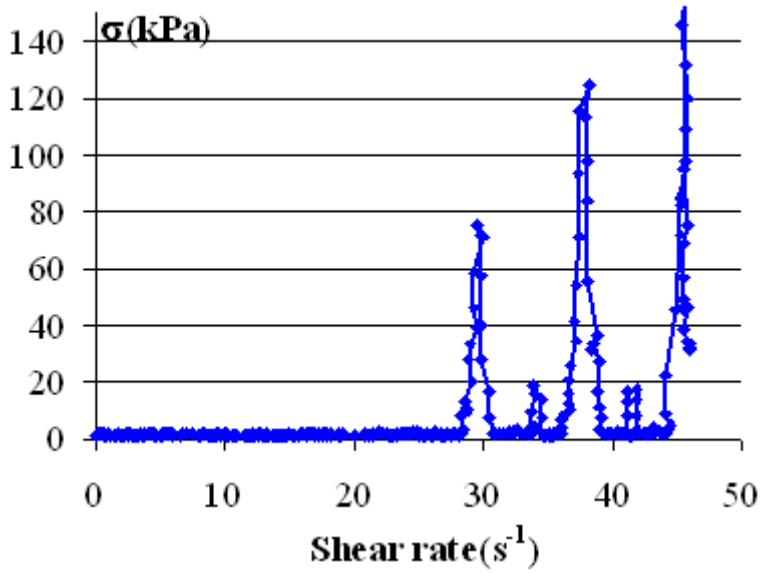

Fig.3b Ramp of shear rate. Iron suspension, Φ=62%

.

Rheological model of the jamming transition

It is now quite well established that the DST is generated by the transition from lubricated to frictional contacts as shown by numerical simulations (20). The key parameter is the fraction of frictional contacts: $f(\sigma)$ which is expected to be a growing function of the stress. It is needed to relate the viscosity to this function; this can be done directly by assuming that the viscosity should diverge when a given fraction of frictional contacts is reached (13) or indirectly by the mean of the volume fraction as proposed in (17). In this last approach two limiting volume fractions are considered corresponding to $f(\sigma)=0$ and $f(\sigma)=1$. The first one Φ_0 corresponds to the maximum packing fraction of the suspension in the absence of frictional contacts. It would be the random close packing $\Phi_0=0.64$ for monodisperse spheres, although the structure formed by the flow can change this diverging volume fraction which can reach 0.7 and may correspond to the stacking of FCC multilayers rafts (21) For polydisperse suspensions it can be much higher, around $\Phi=0.8$ (21). The second critical volume fraction is the one corresponding to the jamming of the actual suspension: Φ_m where all the contacts are frictional and the suspension can no longer flow whatever the stress. Then,

for a given stress, the authors assume that the viscosity will follow the usual law of divergence of the viscosity, but with a maximum volume fraction $\Phi_m<\Phi_j(\sigma)<\Phi_0$;

$$\eta(\sigma)=\eta_0\frac{1}{\left(1-\Phi/\Phi_j(\sigma)\right)^p}\quad \text{with}\quad p=2 \qquad (2)$$

The diverging volume fraction $\Phi j(\sigma)$ must be related to the function $f(\sigma)$ since its two limits correspond to f=0 and f=1 and the simplest hypothesis is a linear dependence :

$$\Phi_j(\sigma)=\Phi_m f(\sigma)+\Phi_0\left(1-f(\sigma)\right) \qquad (3)$$

As $f(\sigma)$ is a growing function of the stress, the maximum packing fraction will decrease with the stress and so the viscosity will increase (cf Eq.(2)). If the viscosity $\eta(\sigma)$ grows faster than σ, then the shear rate $\dot{\gamma}(\sigma)=\sigma/\eta(\sigma)$ will begin to decrease, corresponding to the beginning of the DST transition. We are going to see how this model can be used to reproduce our experimental data. In Fig. 4 we have reported the rheograms obtained on a suspension of carbonyl iron with 0.2% in weight of superplastifier and different volume fractions. At Φ=56% we have a shear thickening behavior followed by a slight "S-shape" characteristic of the DST transition. At Φ=58% the S-shape is more pronounced and at Φ=62% and Φ=64%, the S shape has been replaced by an abrupt decrease of the shear rate followed by an oscillation regime.

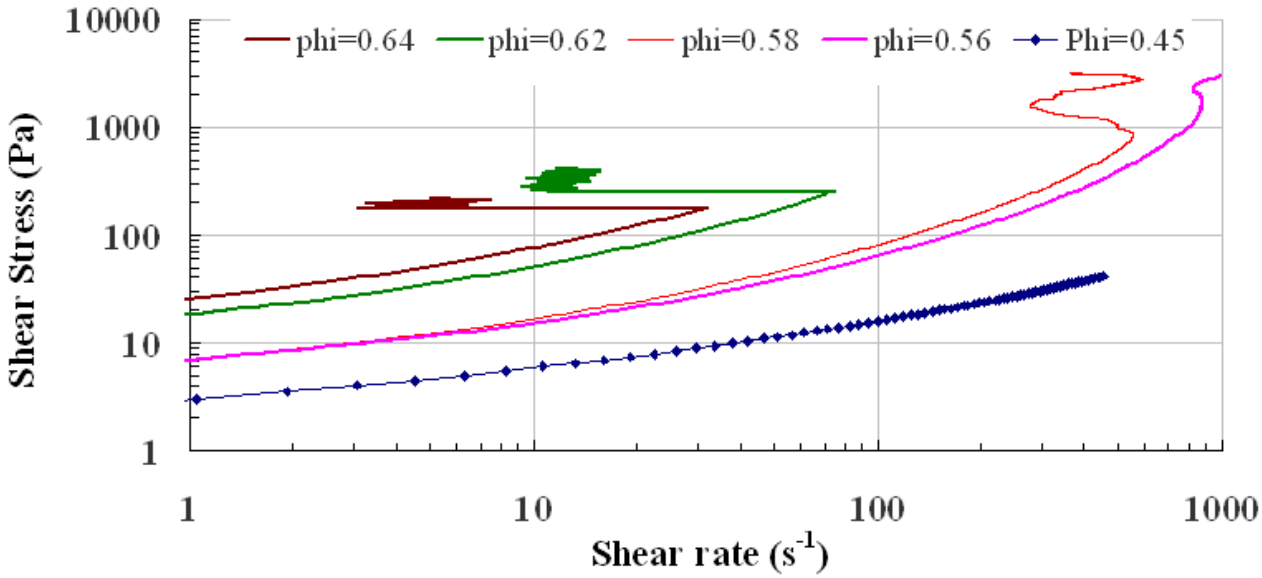

Fig.4 Rheograms of a suspension of carbonyl iron with 0.2%wt of PPP44 for different volume fractions

We are going to fit the curve presenting the characteristic S-shape at Φ=58% with the help of Eqs. (2)-(3). The maximum volume fraction at which the suspension is completely jammed from the beginning is Φ_m=66%. As already discussed, the maximum packing fraction without friction can be taken as Φ_0=0.8 for a polydisperse suspension. The shape of the function $f(\sigma)$ is unknown, it is just a monotonous growing function between 0 and 1. The choice of the simple function: $1-\exp(-\sigma/\sigma_c)$ where σ_c is the critical shear stress can be done (17) but it is convenient to introduce a parameter λ which will determine the steepness of the function and will help to fit the experimental result. In this case we shall have: $f(\sigma)=1-\exp(-\lambda.\sigma/\sigma_c)$. The two remaining parameters λ and η_0 can be obtained by requiring first that the curve passes by the point $(\sigma_c,\dot{\gamma}_c)$ and second that the derivative $\left.\frac{d\dot{\gamma}}{d\sigma}\right|_{\sigma=\sigma_c}=0$ at this point. This last condition links λ to p and it is expressed by:

$$\left(\sigma_c-\tau_y\right)\left.\frac{d\mathrm{Log}(\eta)}{d\sigma}\right|_{\sigma=\sigma_c}=1 \quad\rightarrow\quad \frac{p.\Phi(\Phi_0-\Phi_m)}{\Phi_{jc}\left[\Phi_{jc}-\Phi\right]}\left.\frac{df(\sigma)}{d\sigma}\right|_{\sigma=\sigma_c}=\frac{1}{\sigma_c-\tau_y} \qquad (4)$$

We have introduced the yield stress τ_y which is often found at high volume fraction. Together with Eq. (2), it imposes for the viscosity $\eta(\sigma_c)$ at the critical point to satisfy the Bingham law. In this expression Φ_{jc} is the value of Φ_j for $\sigma=\sigma_c$. It appears that with the value p=2 for the divergence of the viscosity and $f(\sigma)=1-\exp(-\lambda.\sigma/\sigma_c)$, there is no value

of λ which can fulfil Eq.(4) to represent the S shape at Φ=0.58 with the corresponding critical point σ_c=927 Pa and $\dot{\gamma}_c$=536s^{-1}. A more stronger divergence of the viscosity would be needed (p=4) to satisfy Eq. (4). Instead we have used a sigmoid function for f(σ) which allows to satisfy this condition with p=2:

$$f(\sigma) = \frac{1}{1+\exp\left[-\lambda\left(\frac{\sigma}{\sigma_c}-1\right)\right]} \qquad (5)$$

The value of η_0 is fixed by the condition: $$\eta_0 = \frac{\sigma_c - \tau_y}{\dot{\gamma}_c}\left(1-\frac{\Phi}{\Phi_j(\sigma_c)}\right) \qquad (6)$$

In Fig. 5, we have plotted the experimental curves of Fig. 4 for Φ=0.58 and Φ=0.62 together with the theoretical expressions given by Eqs (2), (3) and (5). The values of λ and η_0 obtained from Eqs (4) and (6) are for Φ=0.58: η_0=0.076Pa.s, λ=3.12 and for Φ=0.62: η_0=0.077Pa.s, λ=2.51. The yield stress was taken respectively as 7 Pa and 20 Pa. We first note that the model reproduces qualitatively the S-shape at Φ=0.58 but not at all the abrupt decrease at Φ=0.62. In order to have this abrupt decrease, the viscosity should increase abruptly, but the divergence of the viscosity (Eq.(2)) with $\Phi_j(\sigma)>\Phi_m$=0.67 can't reproduce it because it will smoothly tend towards $\eta_{max}=(1-\Phi/\Phi_m)^{-2}$ and then end up with a Newtonian behavior at high stress as we see on the figure (black solid line). A possible explanation of this failure would be the onset of instability at the turning point. We shall discuss this hypothesis in the third section. Concerning the parameter η_0 it is interesting to note that it remains almost the same for the two volume fraction, but it does not represent the viscosity of the suspending fluid, that in our case is equal to 0.08Pa.s

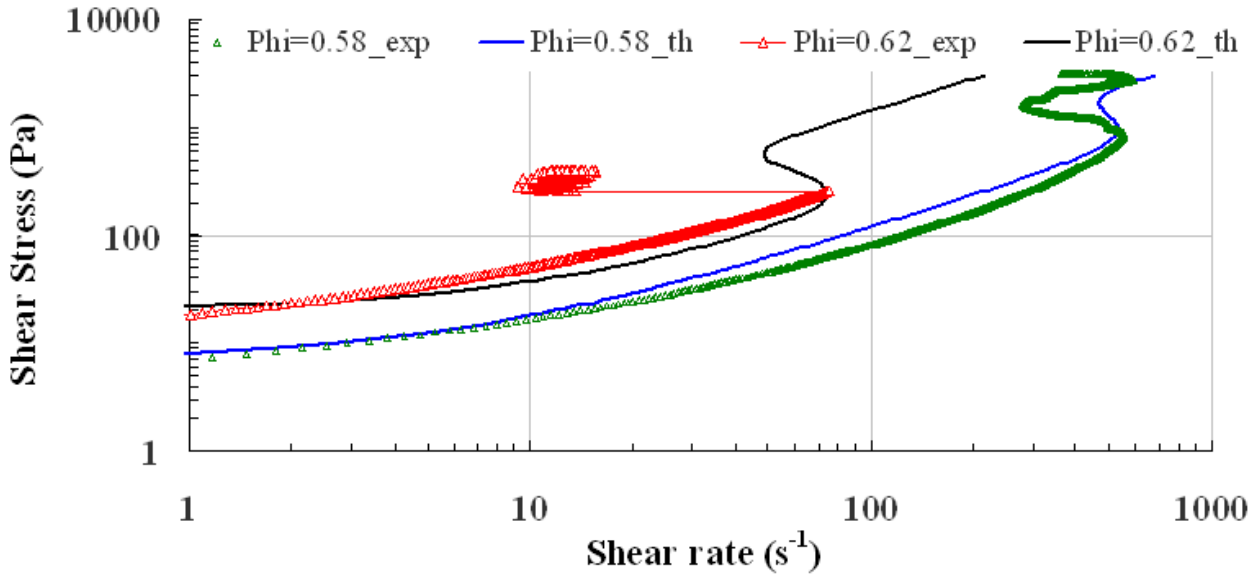

Fig.5 Fit of the experimental rheograms with the Eqs(2),(3),(5)for Φ=0.58 (blue solid line) and Φ=0.62 (black solid line)

Effect of a magnetic field on the jamming transition

The jamming transition is provoked by the failure of the repulsive coating layer, adsorbed on the particles to prevent a direct contact between the surfaces,above a given applied stress. The applied stress is a key parameter since we expect that the force which pushes two particles against each other will behave like: $F_a = \pi a^2 \sigma_a$ where σ_a is the applied stress. Above a given applied force we suppose that the compression of the polymer layer is large enough to be able to push away the molecules adsorbed on the surface, and then to induce the transition from a lubricated to a frictional regime. So for $\sigma_a>\sigma_c$ the transition should occur. If we add an external attractive force between the particles, such as a magnetic force, we could expect that the transition will take place at a lower hydrodynamic stress

, σ_h ,since we have now the condition $\sigma_h + \tau_y > \sigma_c$ where τ_y is the magnetic stress which is approximately equivalent to the yield stress due to the application of the magnetic field (22), (23). Then the condition:

$$\eta_0 \frac{1}{\left(1-\Phi/\Phi_j(\sigma_c)\right)^2}\ \dot{\gamma}_c + \tau_y = \sigma_c \qquad (7)$$

states that if τ_y increases the critical shear rate should decrease, at least if $\Phi_j(\sigma_c)$ does not vary too much with the magnetic field. This is what we observe in Fig. 6 where we present a complete sweep of amplitudes of magnetic field for a volume fraction of carbonyl iron particles with Φ=63% suspended in a mixture of water and ethylene glycol. In these experiments we have used a plate-plate geometry and the field is perpendicular to the surface of the rotating disk.

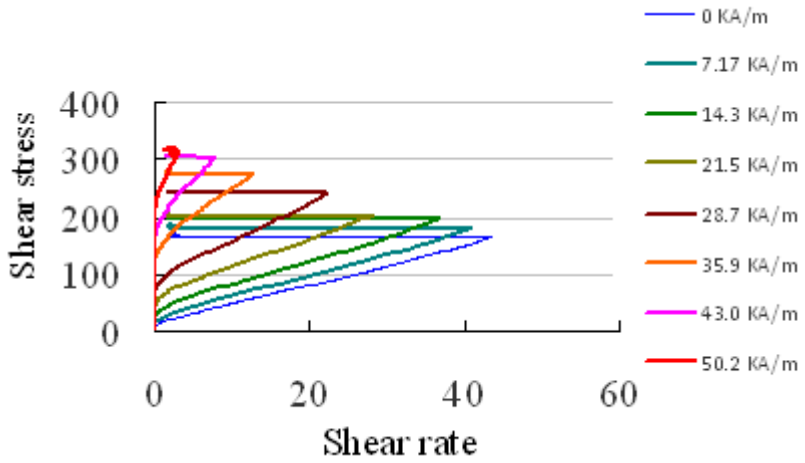

Fig.6 Ramp of stress for different amplitudes of magnetic field Φ=63%. A magnetic field of 10kA/m is equivalent to an induction of 12.5 10^{-3} Tesla

We actually observe the decrease of the critical shear rate as the amplitude of the magnetic field increases and also a regular increase of the critical stress σ_c. In the two following figures we have reported (Fig 7a) the critical stress corresponding to Fig.6 and the difference between the critical stress and the yield stress (Fig.7b). We observe in fig.7a that the final critical stress is about two times the initial one. On the other hand, if we subtract the yield stress from the critical one in order to keep only the hydrodynamic component of the stress, then this component does not increase with the magnetic field (Fig.7b). It indicates that it is the hydrodynamic component which drives the jamming transition, the magnetic one just modify the yield stress and the dynamic viscosity of the suspension (since the slope of the curve increases steadily with the field) but does not contribute directly to the force which will sweep out the coating polymer.

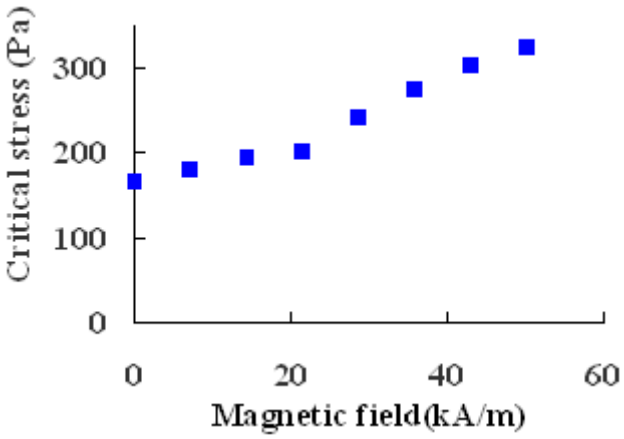

Fig.7a Critical stress of the jamming transition versus the applied magnetic field for Φ=63%

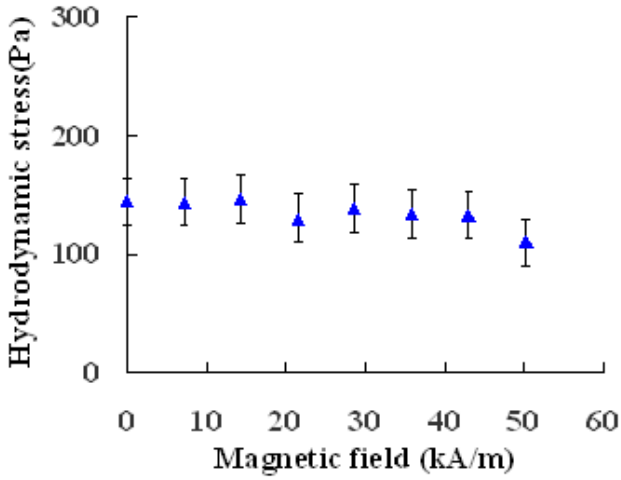

Fig7b The critical stress minus the yield stress for the same experiment than in Fig.7a

In other words, it means that it is not so much the compression of the polymer layer that is needed to get rid of it but rather a shear force which is provided by the hydrodynamic stress. If it was a compression force which was required to remove the polymer then since both the magnetic and the hydrodynamic one contribute to the compression, the critical stress should remain constant instead of increasing as shown in Fig. 7a.
Another interesting situation is obtained if we impose a given shear rate and raise the magnetic field. The result of this experiment is shown in Fig. 8.

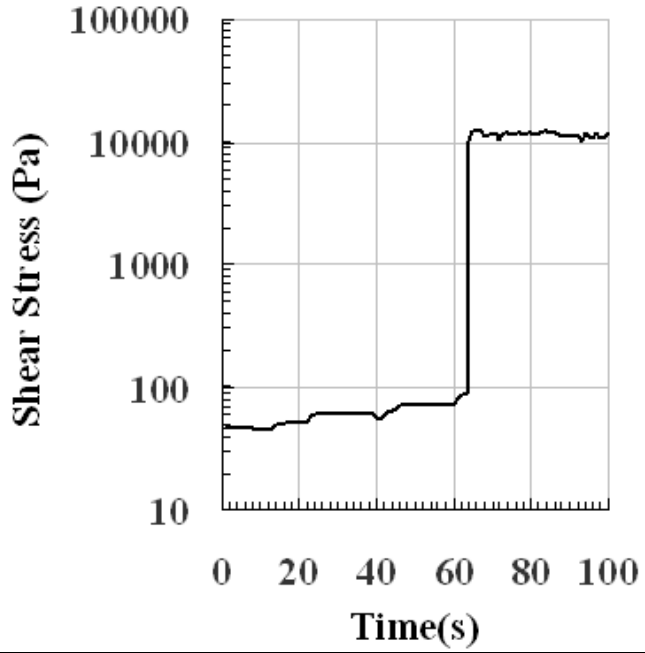

Fig.8 Increase of the field step by step at a constant shear rate of $30s^{-1}$. Volume fraction Φ=0.61

A shear rate of $30s^{-1}$ was applied from the beginning. and we raised progressively the amplitude of the magnetic field. The jump of stress occurs a few second after the step of 21kA/m. The jump of stress corresponds to two orders of magnitude, and is actually limited by the maximum torque of the rheometer (here 0.3N.m). Using the homemade rheometer with the cell shown in fig. 3a, we found that the yield stress can jump up to 150kPa for field of only 8kA/m. Furthermore, instead of oscillating between a jammed state and a flowing state as it is the case in the absence of field (cf Fig. 3b), it remains in the jammed state (24) which allows to use this field induced jamming transition for applications in force or torque transmission.
We have seen that above the jamming transition we observe large fluctuations of the shear rate during a ramp of stress (Fig. 2) or of the stress during a ramp of shear rate (Fig. 3b). We are now going to analyse more specifically this instability which occurs above the critical point both in absence and in presence of a magnetic field

Analysis of the instabilities above the jamming transition

No magnetic field

Contrarily to what is observed with cornstarch suspensions or some silica suspensions where we have a soft transition which manifests by a S-shape, as is the case also at the lowest volume fraction (cf Fig. 4), we have here an immediate decrease of the shear rate followed by a regime of strong oscillations (cf Fig.1-2). Some of them were observed at imposed shear rate (8), and imposed stress (25), (26) in shear thickening suspensions. If we conduct an experiment at a fixed stress above the critical one in a plate-plate geometry, we see in Fig. (9) that we have some regular oscillations with a saw tooth shape. At the lowest stress, just above the transition, the shear rate can even change of sign as we previously observed in calcium carbonate suspensions (13), meaning that the rotational velocity of the upper disk is inverted during a short interval of time. The second observation is that, at higher imposed stress, the oscillations are of smaller amplitude and of higher frequency. We previously (13) gave an explanation of these oscillations with a saw tooth shape by introducing the inertia of the tool in the equation of motion in the presence of a rheological model presenting a S-shape but with a simple equilibrium model where the viscosity was supposed to diverge as $\eta(f)=\eta_0 (f-f_M)^{-p}$ where f_M was a parameter. We are now reconsidering this model with the viscosity represented by Eqs (2), (3). We are also including the yield stress, τ_y in the two dynamical equations for the stress and the fraction of frictional contacts:

$$\frac{I}{C}\ddot{\gamma}(t) = \sigma_a(t) - \eta(f(t))\dot{\gamma}(t) - \tau_y \qquad \text{or:} \qquad \sigma_s(t) = \sigma_a(t) - \frac{I}{C}\ddot{\gamma}(t) = \eta(f(t))\dot{\gamma}(t) + \tau_y \tag{8}$$

$$\frac{\partial f}{\partial t} = -\frac{1}{\tau}(f - f_e(\sigma_s)) \tag{9}$$

In Eq. (8) $I=9.36\ 10^{-5}$ is the inertia of the tool plus the one of the motor which is attached on the same axis and $C=\Box R^4/2h = 2.51\ 10^{-4}$ is a constant specific to the plate-plate geometry having a gap h =1mm and a radius R=20mm. The term: $\Box dv/dt$ expressing the inertia of the suspension does not appear since it is negligible compared to the mechanical inertia. Nevertheless; this term which gives a spatially variable stress, is responsible also for an instability but at much higher frequencies (27) than those appearing in Fig (9).

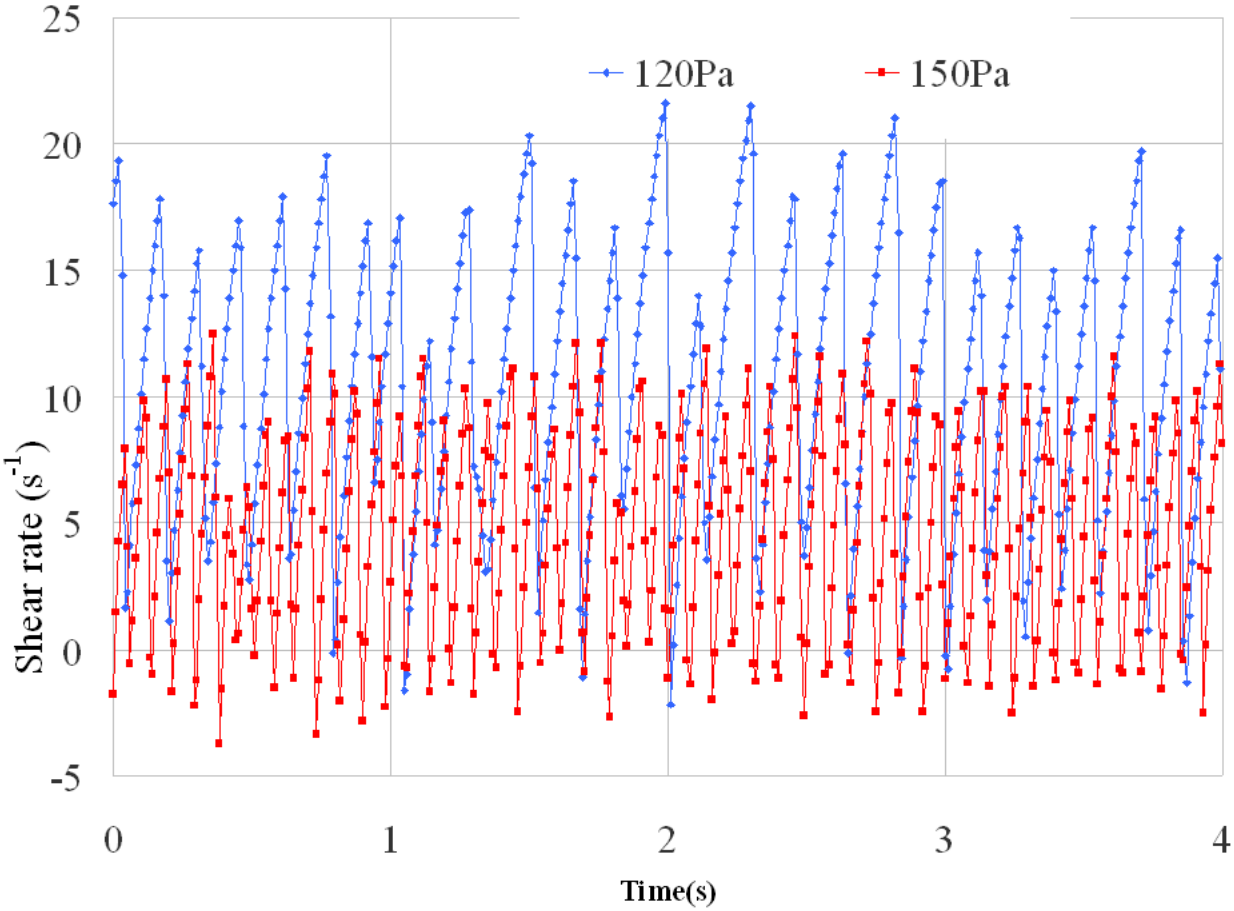

Fig.9 Shear rate versus time for a constant applied stress of 120 Pa and then 150Pa. Carbony iron suspension at Φ=0.62 with 0.2% weight of PPP44

An important point is that the real stress acting on the suspension is not the supposed applied one but the applied one plus the one coming from the inertia of the tool as was demonstrated in (26). Consequently the fraction of frictional contacts should depend on the actual stress:σ_s which is different from the applied stress, σ_a, because of the inertia term given by Eq. (8). The yield stress τ_y introduced in this Eq. (8) can arise from any attractive force including the magnetic one and a generalization of σ_m in Eq. (7).
We can apply a linear stability analysis to Eqs. (8) and (9) in order to predict the frequency of the oscillations. The perturbations are givens in the usual way: with respect to the equilibrium values:

$$f = f_e(\sigma_a) + \delta f \qquad \dot{\gamma} = \dot{\gamma}_a + \delta\dot{\gamma} \qquad \text{with } \delta f = A.e^{\Omega.t} \text{ and } \delta\dot{\gamma} = B.e^{\Omega.t} \tag{10}$$

The viscosity is a function of f through the equations (2) and (3) and needs to be developed as:

$$\eta(f)=\eta(f_e)+\left.\frac{\partial\eta}{\partial f}\right|_{f_e}\delta f \qquad \text{and we have also} \qquad f_e(\sigma_s)=f_e(\sigma_a)+(\sigma_s\ddot{}-\sigma_a)\left.\frac{\partial f}{\partial\sigma}\right|_{\sigma_a} \qquad (11)$$

Taking into account that (cf Eq. (8)) : $\sigma_s-\sigma_a=-(I/C)\ddot{\gamma}$ and that $\ddot{\gamma}=\delta\ddot{\gamma}$ since $\ddot{\gamma}_e=0$ at equilibrium, and inserting Eqs. (10) and (11) into Eqs (8) and (9), we end up, after keeping only the linear terms in the perturbation, with:

$$\left[\frac{I}{C}\Omega+\eta(\sigma_a)\right]\delta\dot{\gamma}+\dot{\gamma}_a\left.\frac{\partial\eta}{\partial f}\right|_{\sigma_a}\delta f=0 \qquad \text{and} \qquad \frac{I}{C}\left.\frac{\partial f}{\partial\sigma}\right|_{\sigma_a}\Omega\,\delta\dot{\gamma}+(1+\tau\Omega)\delta f=0 \qquad (12)$$

The condition of a zero discriminant of these two equations gives the following equation for Ω:

$$\Omega^2+\Omega\left[\frac{1}{\tau_I(\sigma_a)}+\frac{\eta(\sigma_a)}{\tau}\left.\frac{\partial\dot{\gamma}}{\partial\sigma}\right|_{\sigma_a}\right]+\frac{1}{\tau\,\tau_I}=0 \qquad \text{with} \qquad \tau_I(\sigma_a)=\frac{I}{C.\eta(\sigma_a)}=\frac{I}{\eta(\sigma_a)}\frac{2h}{\pi R^4} \qquad (13)$$

where τ_I is the inertial time which depends strongly on the radius of the upper disk. To derive Eq. (13) we have used:

$$\left.\frac{\partial\eta}{\partial f}\right|_{\sigma_a}\left.\frac{\partial f}{\partial\sigma}\right|_{\sigma_a}=\left.\frac{\partial\eta}{\partial\sigma}\right|_{\sigma_a}=\frac{1}{\dot{\gamma}_a}\left[1-\frac{\eta(\sigma_a)}{\tau}\left.\frac{\partial\dot{\gamma}}{\partial\sigma}\right|_{\sigma_a}\right]$$

In these equations σ_a is the applied stress and $\dot{\gamma}_a$ the corresponding shear rate in the absence of instability. The result for the angular frequency is then:

$$\Omega=0.5\left[\ddot{}-\left(\frac{1}{\tau_I(\sigma_a)}+\frac{\eta(\sigma_a)}{\tau}\left.\frac{\partial\dot{\gamma}}{\partial\sigma}\right|_{\sigma_a}\right)\pm\sqrt{\left(\frac{1}{\tau_I(\sigma_a)}+\frac{\eta(\sigma_a)}{\tau}\left.\frac{\partial\dot{\gamma}}{\partial\sigma}\right|_{\sigma_a}\right)^2-\frac{4}{\tau.\tau_I(\sigma_a)}}\right] \qquad (14)$$

If the first term becomes negative then the term exp(Ωt) diverges and we have the growth of the instability whose period is given by :

$$T=2\pi/\Omega_c=2\pi\sqrt{\tau.\tau_I(\sigma_c)} \qquad (15)$$

In principle, we see that the parameter τ describing the rate at which the percolation fraction returns to its equilibrium value can be deduced from the experimental period of the oscillations. We have compared in Figs.10 and 11 the predictions of the dynamical model (Eqs 8-9) both for the ramp of stress and for the two stationary values of 120 Pa and 150 Pa which are above the critical stress σ_c=97Pa. In Figs.9-11 the experimental curves correspond to the same suspension of carbonyl iron in water at Φ=62% with 0.2% of superplastifier

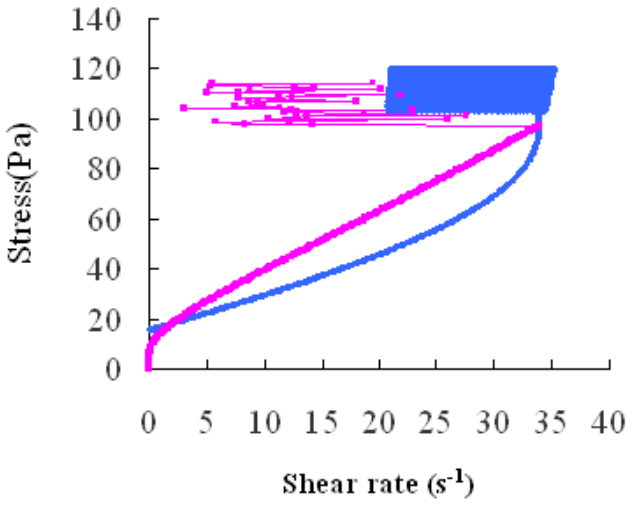

Fig.(10) Φ= 62% iron particles in water with 0.2% PPP44. Purple experimental shear rate versus applied

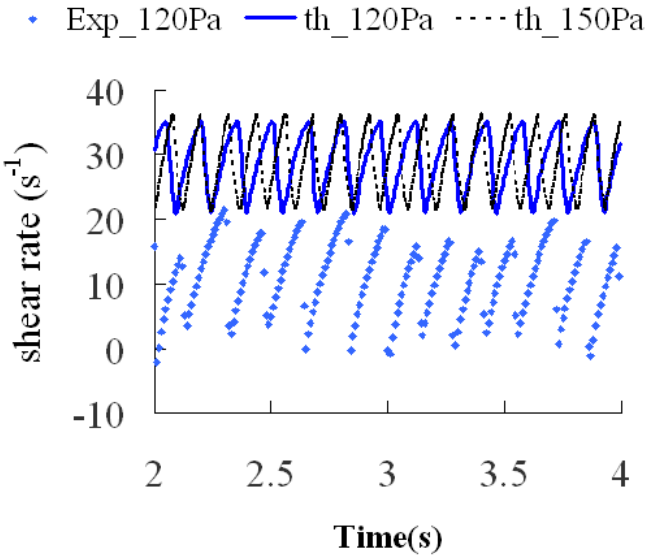

Fig.(11) Oscillations of shear rate at constant applied stress. Blue losange: experiment at 120Pa. Solid blue line:model at

stress . Blue: Model with Eqs(8)-(9). 120Pa. Black dotted line:model at 150Pa

In Fig. (10), the theoretical curve (in blue) was obtained with τ_y=15Pa ; λ=2.48 for the sigmoid (Eq. (5)) and η_0=0.059 for the viscosity (Eq. (2)).These two last values are those which match the critical point to the experimental one obtained with Eqs.(4) and (6). We can see that, given these constraints at $\dot{\gamma}=0$ and at $\dot{\gamma}=\dot{\gamma}_c=34s^{-1}$, the theoretical curve is quite different from the experimental one. Actually the theoretical model is based on a progressive shear thickening before the DST transition since the jamming volume fraction $\Phi_j(\sigma)$ decreases continuously when σ increases, which results in an increasing viscosity with σ. On the contrary the experiment (purple curve in Fig.10) can be represented by a Bingham law up to the transition point, meaning that the fraction of percolating contacts remains low and suddenly increases at the critical stress. As in the experiment, above the critical stress, we obtain strong oscillations of the shear rate, but with two differences: the amplitude of these oscillations is smaller than in the experiment and their maximum value remains close or slightly above $\dot{\gamma}_c$. This is more visible in Fig.(11) where we have plotted the experimental oscillations of the shear rate for a constant applied stress of 120 Pa (blue losanges) together with the prediction of the model (solid blue line). We see that the theoretical oscillations are well above the experimental ones. In order to get the same period as the experimental one: T_{exp}=0.16s we have taken τ=2ms. The theoretical period given by Eq. (15) with τ=2ms is slightly smaller: T_{th}=0.11s, this is not surprising because it comes from a linear approximation valid when the instability just begins to develop.

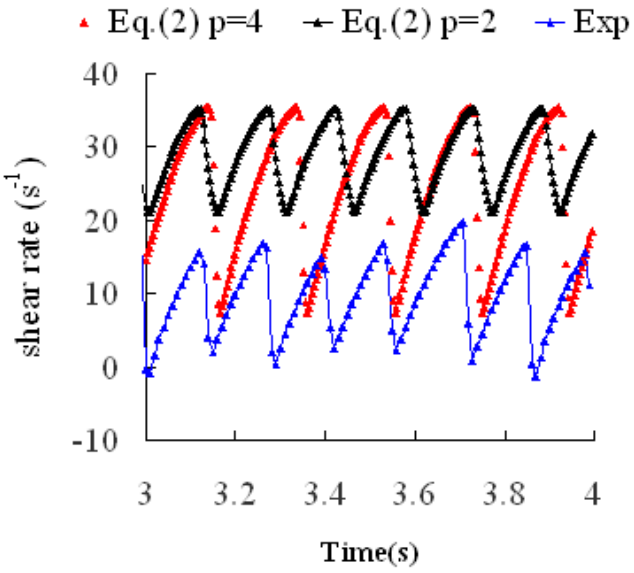

Fig(12) Comparison of two divergences of the viscosity (Eq.(2)) witheither p=2 (black triangles) or p=4 (red triangles) The blue triangles are tfrom experiment.

At last we see in Fig. 11 that for a higher stress σ=150 Pa the period of the oscillation has slightly decreased:(black dotted line) with T_{th}=0.12s. This is coherent with the experimental observation (cf Fig. (9)) although the decrease is more pronounced with T_{exp}=0.083s. Qualitatively, this decrease of the period is related to the decrease of $\tau_I(\sigma)$ (Eqs (13) and (15)) since the viscosity increases with the stress

In order to reproduce the large value of the oscillations observed in Fig. (9), it is needed to use a different model for the divergence of the viscosity like the one used in (13). For instance in Fig. (12) we have used a stronger divergence of the viscosity with p=4 instead of p=2. Comparing the black curve to the red one we see that the amplitude of the oscillations is increased and, also that the drop of the shear rate is more abrupt like the one of the experimental curve (blue triangle). Nevertheless the major difference with the experimental curve is that the upper value of the shear rate remains close to the critical one whereas in the experiments, after the abrupt recoil of the shear rate, the oscillations never reach again the critical one (cf Fig. 10). The fact to use p=4 in Eq. (2) for the viscosity has no theoretical justification, it just emphasizes the need for a more abrupt increase of the viscosity with the stress or in other words to generate a stronger negative slope in the S-shape of the stress versus shear rate curve. We believe that, since the jamming transition generates a frictional stress, there is no reason to stick to a dependence of the viscosity which is only justified in the presence of lubrication and soft repulsive forces.

In (13) we took $\eta(f)=\eta_0\,(f(\sigma)-f_M)^{-p}$ which is somewhat arbitrary but takes into account that the divergence of the viscosity is directly driven by a critical fraction of frictional contacts rather than by a critical volume fraction, even if this critical fraction should be a function of the volume fraction of the suspension.

Influence of a magnetic field on the oscillating regime

As we have seen previously in Fig.(6) the application of a magnetic field allows to decrease the critical shear rate of the jamming transition. We are going to investigate the effect of the magnetic field on the oscillation regime above the transition. This effect is shown in Fig.(13) where we have increased step by step the magnetic field ,keeping constant the applied stress, always at a volume fraction of 62%. The oscillations of the shear rate quickly decreases when we increase the field and their frequency increases. Then their shape becomes more irregular and finally above 10kA/m they have totally disappeared (solid green line).

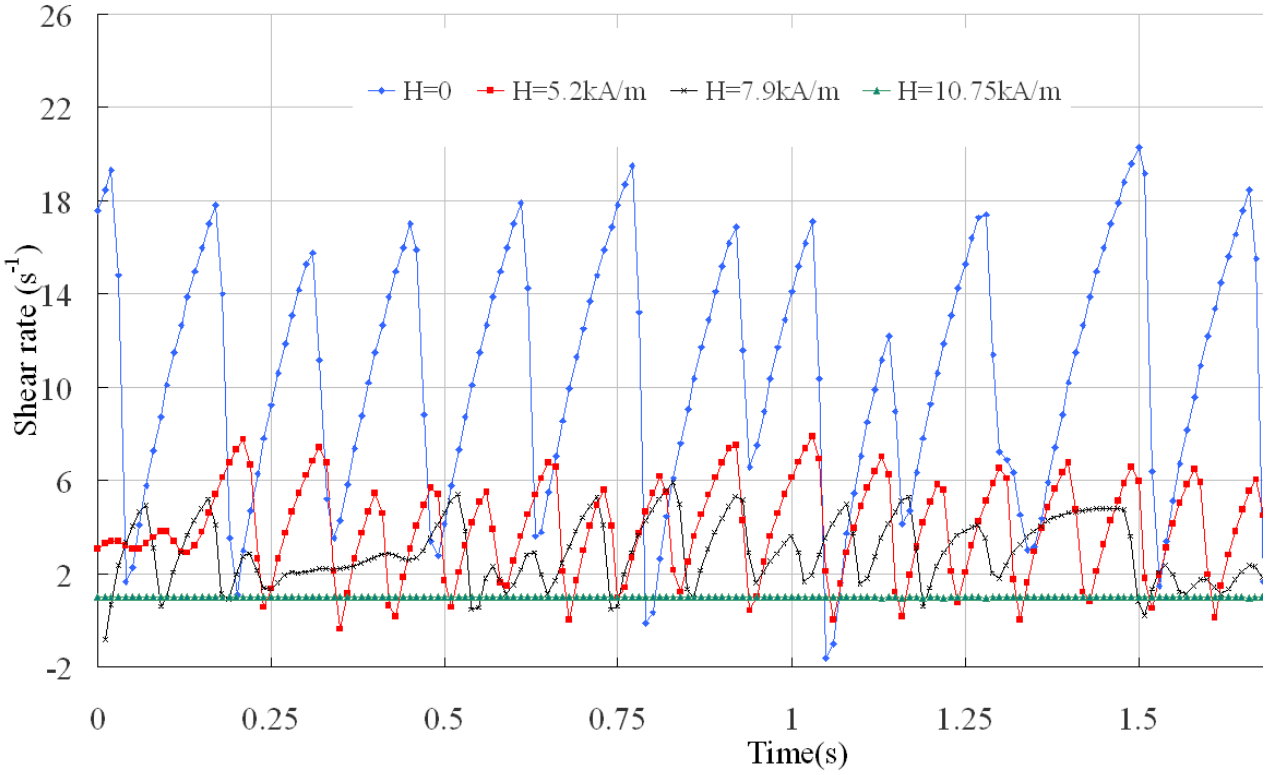

Fig. (13) Oscillating regime for the shear rate at constant applied stress: σ_a=120Pa, for differents magnetic fields. Volume fraction of carbonyl iron Φ=62%

Actually, as shown in Fig. (6),when we increase the magnetic field we also increase the critical stress above which the instability appears. It is then understandable that, if we apply a constant stress (here 120 Pa) and increase the magnetic field, the critical stress will go above the applied one and we shall fall inside the stable region, so the instability will disappear. Nevertheless, if we apply the model described above by increasing progressively the critical stress in order to represent he effect of the magnetic field ,we do not observe the same behavior as the one described in Fig. (13): the amplitude and the frequency of oscillations remain practically constant until a critical stress of 119.5Pa is reached where the oscillations suddenly disappear. Once again it appears that the description of the evolution of the viscosity with the stress (Eqs. (2)-(3)-(5)) is not well adapted to systems where the fraction of frictional contacts vary abruptly with the stress.

Jamming transition in a capillary

Until now, we have considered rotational geometries, but in many industrial processes like the injection of pastes or ceramics inside molds, the suspension is pushed inside a capillary, so it is important to see how this jamming transition behave in a capillary. To achieve this aim, we have used a Malvern RH7 capillary rheometer whose diameter of the barrel was 9.5mm and its length 28 mm. The diameter of the capillary was d=2R= 0.75mm and its length L=3mm. The pressure sensor was placed inside a hole perpendicular to the axis of the barrel and close to its end where the capillary is screwed.
For a viscous medium, the shear rate at the wall of the capillary and the pressure drop are respectively given by:

$$\dot{\gamma} = 4Q/(\pi R^3) \quad \text{and} \quad P_{vis} = 8L\,\eta\,Q/(\pi R^4) \tag{16}$$

Where η is the viscosity of the suspension, Q the flow rate and L the length of the capillary. The experiment was done with a volume fraction of iron Φ=64% in a mixture of ethylene glycol and water always with 0.2% of superplastifier. The viscosity of the suspension was η= 5.4Pa.s. The pressure versus the shear rate is represented in Fig. 14a for two different ramps of shear rate.

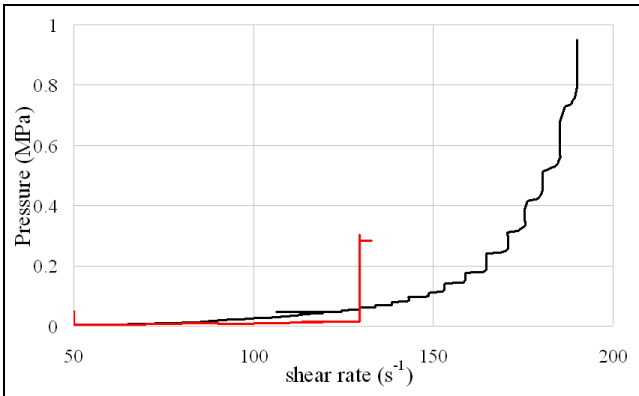

Fig.(14a) Pressure versus shear rate in a capillary rheometer. Suspension of iron Φ=64%. Red curve :slow increase of shear rate (see Fig 13b).
Black curve:fast increase ($60s^{-1}$/mn)

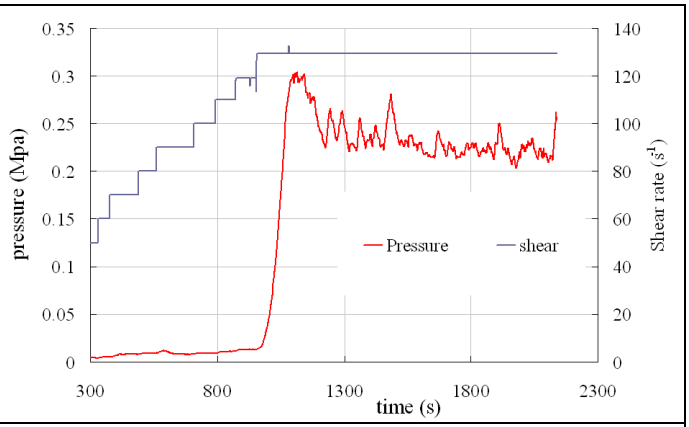

Fig. (14b) : Evolution of shear rate (blue curve) and of the pressure(red curve) with time. It corresponds to the red curve of the left figure.

The first one corresponds to a ramp with a constant shear rate of $50s^{-1}$ during 300s and then a ramp from $50s^{-1}$ to 300 s^{-1} in 700s; the second one to a ramp of shear rate from 0 to $180s^{-1}$ in 175s. In Fig. 14b we have plotted, for the slow ramp, the pressure and the shear rate versus time. We can observe that, when the shear rate is raised slowly, we have an abrupt transition at the last step of shear rate with the pressure rising from 0.02MPa to 0.3MPa .This is the signature of a jamming transition otherwise the pressure should vary linearly with the shear rate (cf Eq. (16)). After this peak, if the shear rate is kept constant, the pressure decreases slightly and fluctuates around 0.22MPa. If, on the contrary, we increase the shear rate more rapidly, then we still observe an increase of pressure which is not at all linear with time but does not show this abrupt transition. The pressure steps observed in Fig. 14a (black line) correspond to the shear rate steps. If we calculate the pressure at the maximum shear rate of $130s^{-1}$ from Eq. (16), that is to say for the flow of a viscous suspension, we obtain a pressure drop of 0.011 MPa instead of 0.22 MPa. It means that we no longer have a suspension flowing in the capillary, but a less concentrated suspension flowing through a jammed skeleton of particles forming a porous media. Although it is not related to a jamming transition, this phenomenon is well known in extrusion of pastes where a plug of solid particles is formed and the liquid of the suspension filtrates through this porous plug (28), (29). It was also studied in suspensions of PMMA particles, with a suspending liquid of about the same refractive index in order to visualize the flow, which was sucked inside a syringe (30). If instead of a viscous flow we consider a flow of the suspending liquid through a porous medium made of a network of the solid particles ,the pressure drop can be obtained from the Carman-Kozeny equation:

$$P_{por} = L.\mu.\frac{Q}{\pi.R^2}\frac{1}{K} \quad \text{with} \quad K = \frac{\varepsilon^3 d^2}{180(1-\varepsilon)^2} \qquad (17)$$

K is the Carman-Kozeny constant for a bed of spherical particles of diameter d; $\varepsilon=1-\Phi$ is the porosity and μ the viscosity of the suspending fluid. For the maximum shear rate, we have now P_{por}=2190MPa. This is much bigger than the observed pressure. A possible explanation is that the jamming does not occur inside the capillary but rather before its entrance (28), so the superficial velocity $Q/(\pi R^2)$ and the filtration pressure would be much lower than predicted by Eq. (17) since R is no longer the radius of the capillary but rather the radius of the barrel. Even in this case it is still higher than the experimental one:P_{barrel}=13.6MPa meaning that this porous media is not consolidated. It is also coherent with the high value of the critical shear rate: $\dot{\gamma} \approx 130\ s^{-1}$ with respect to the one obtained in rotational geometry which is around $30s^{-1}$, meaning that the jamming does not occur in the capillary. The fluctuations of pressure observed at constant shear rate are likely produced by the intermittent collapse of jammed structure at the entrance of the die as observed in (28).

Conclusion

In this paper we have presented experimental results showing a strong discontinuous shear thickening obtained with a suspension of carbonyl iron particles in the presence of a superplastifier molecule. The jump of stress at imposed velocity can reach more than 100kPa. The model proposed in (17) can reproduce the S-shape observed at the lowest volume fraction, but in this model the transition is preceded by a shear thickening behavior that is practically absent in our experiments at high volume fraction. Introducing a relaxation time,τ, for the fraction of frictional contacts and

the inertia of the tool used in rotational rheometry has allowed to recover the right frequency of the oscillations with only one supplementary parameter: τ. A linear stability analysis show that the period of the oscillations is simply related to the square root of the product of τ and of the inertia time (Eq. 15) allowing to obtain directly this relaxation time from the experimental period. The amplitude of the oscillations obtained with the model of Wyart and Cates (17) appears too small. In order to reproduce both the amplitude and the shape of these oscillations a stronger dependence of the viscosity with the stress is needed. The jamming transition of this suspension of iron particles is very sensitive to the application of a magnetic field and the critical shear rate decreases quickly with the amplitude of the magnetic field, but simultaneously the critical stress increases. Nevertheless, if we subtract the magnetic stress to the applied one, the difference remains constant, indicating that it is the hydrodynamic stress which drives the jamming transition. We also have found that this jamming transition also occurs in capillaries and manifests itself by the building of a porous media constituted of particles in frictional contact. The dynamics of this transition is much slower than in rotational geometry and is likely related to the formation of a plug at the entrance of the die. Further investigations, especially in the presence of a magnetic field, is needed to understand the dynamics of formation of this plug and the influence of the sedimentation on its time of formation. Depending on these results, we can emphasize several applications based on the control of the pressure at imposed flow rate or of the flow rate at imposed pressure, with a small magnetic field.

Acknowledgments

This work was supported by the Centre National d'Etudes Spatiales CNES.

References

1. Quemada D. Rheological modelling of complex fluids: II. Shear thickening behavior due to shear induced flocculation. The European Physical Journal-Applied Physics. 1998;2(2):175–181.

2. Quemada D, Berli C. Energy of interaction in colloids and its implications in rheological modeling. Advances in colloid and interface science. 2002;98(1):51–85.

3. Bossis G, Brady JF. The rheology of Brownian suspensions. The Journal of chemical physics. 1989;91(3):1866–1874.

4. Hoffman RL. Discontinuous and dilatant viscosity behavior in concentrated suspensions. I. Observation of a flow instability. Transactions of the Society of Rheology. 1972;16(1):155–173.

5. Hoffman RL. Discontinuous and dilatant viscosity behavior in concentrated suspensions III. Necessary conditions for their occurrence in viscometric flows. Advances in colloid and interface science. 1982;17(1):161–184.

6. Brown E, Jaeger HM. The role of dilation and confining stresses in shear thickening of dense suspensions. Journal of Rheology. 2012;56(4):875–923.

7. Fall A, Bertrand F, Hautemayou D, Mézière C, Moucheront P, Lemaitre A, et al. Macroscopic discontinuous shear thickening versus local shear jamming in cornstarch. Physical review letters. 2015;114(9):098301.

8. Lootens D, Van Damme H, Hébraud P. Giant stress fluctuations at the jamming transition. Physical review letters. 2003;90(17):178301.

9. Franks GV, Zhou Z, Duin NJ, Boger DV. Effect of interparticle forces on shear thickening of oxide suspensions. Journal of Rheology. 2000;44(4):759–779.

10. Neuville M, Bossis G, Persello J, Volkova O, Boustingorry P, Mosquet M. Rheology of a gypsum suspension in the presence of different superplasticizers. Journal of rheology. 2012;56(2):435–451.

11. Guy BM, Hermes M, Poon WC. Towards a unified description of the rheology of hard-particle suspensions. Physical review letters. 2015;115(8):088304.

12. Egres RG, Wagner NJ. The rheology and microstructure of acicular precipitated calcium carbonate colloidal suspensions through the shear thickening transition. Journal of rheology. 2005;49(3):719–746.

13. Bossis G, Boustingorry P, Grasselli Y, Meunier A, Morini R, Zubarev A, et al. Discontinuous shear thickening in the presence of polymers adsorbed on the surface of calcium carbonate particles. Rheologica Acta. 2017;56(5):415–430.

14. Mari R, Seto R, Morris JF, Denn MM. Shear thickening, frictionless and frictional rheologies in non-Brownian suspensions. Journal of Rheology. 2014;58(6):1693–1724.

15. Comtet J, Chatté G, Niguès A, Bocquet L, Siria A, Colin A. Pairwise frictional profile between particles determines discontinuous shear thickening transition in non-colloidal suspensions. Nature communications. 2017;8:15633.

16. Bossis G, Grasselli Y, Meunier A, Volkova O. Outstanding magnetorheological effect based on discontinuous shear thickening in the presence of a superplastifier molecule. Applied Physics Letters. 2016;109(11):111902.

17. Wyart M, Cates ME. Discontinuous shear thickening without inertia in dense non-Brownian suspensions. Physical review letters. 2014;112(9):098302.

18. Brown E, Jaeger HM. Dynamic jamming point for shear thickening suspensions. Physical review letters. 2009;103(8):086001.

19. Cates ME, Haw MD, Holmes CB. Dilatancy, jamming, and the physics of granulation. Journal of Physics: Condensed Matter. 2005;17(24):S2517.

20. Seto R, Mari R, Morris JF, Denn MM. Discontinuous shear thickening of frictional hard-sphere suspensions. Physical review letters. 2013;111(21):218301.

21. Farr RS, Groot RD. Close packing density of polydisperse hard spheres. The Journal of chemical physics. 2009;131(24):244104.

22. Ginder JM, Davis LC, Elie LD. Rheology of magnetorheological fluids: models and measurements. Int J Mod Phys B. 30 oct 1996;10(23n24):3293‑303.

23. Bossis G, Volkova O, Lacis S, Meunier A. Magnetorheology: fluids, structures and rheology. In: Ferrofluids. Springer; 2002. p. 202–230.

24. Bossis G, Grasselli Y, Meunier A, Volkova O. Tunable discontinuous shear thickening with magnetorheological suspensions. Journal of Intelligent Material Systems and Structures. 1 janv 2018;29(1):5‑11.

25. Nagahiro S, Nakanishi H, Mitarai N. Experimental observation of shear thickening oscillation. EPL. 2013;104(2):28002.

26. Larsen RJ, Kim J-W, Zukoski CF, Weitz DA. Fluctuations in flow produced by competition between apparent wall slip and dilatancy. Rheol Acta. 1 avr 2014;53(4):333‑47.

27. Nakanishi H, Nagahiro S, Mitarai N. Fluid dynamics of dilatant fluids. Phys Rev E. 11 janv 2012;85(1):011401.

28. Khelifi H, Perrot A, Lecompte T, Rangeard D, Ausias G. Prediction of extrusion load and liquid phase filtration during ram extrusion of high solid volume fraction pastes. Powder Technology. 1 nov 2013;249:258‑68.

29. Rough SL, Bridgwater J, Wilson DI. Effects of liquid phase migration on extrusion of microcrystalline cellulose pastes. International Journal of Pharmaceutics. 20 juin 2000;204(1):117‑26.

30. Haw MD. Jamming, Two-Fluid Behavior, and ``Self-Filtration'' in Concentrated Particulate Suspensions. Phys Rev Lett. 5 mai 2004;92(18):185506.

Figure and table captions
Table and figure captions should be included at the end of the manuscript file and should be brief and informative. Ensure that permission has been obtained for all use of third party or previously published figures, and include full credit information. If publishing an open access paper, permission must be cleared for this use. Please let the Editorial Office know of any copyright issues.

Figures
For final submissions, figures should be uploaded as separate, high resolution, figure files.